Dalton Transactions

PAPER

View Article Online
View Journal | View Issue

Cite this: *Dalton Trans.*, 2015, **44**, 8649

Inducing magnetic communication in caged dinuclear Co(II) systems†

Judith Caballero-Jiménez,[a] Fatemah Habib,[b] Daniel Ramírez-Rosales,[c] Rafael Grande-Aztatzi,[d] Gabriel Merino,[d] Ilia Korobkov,[b] Mukesh Kumar Singh,[e] Gopalan Rajaraman,[e] Yasmi Reyes-Ortega[a] and Muralee Murugesu*[b]

Received 3rd February 2015,
Accepted 26th March 2015

DOI: 10.1039/c5dt00497g

www.rsc.org/dalton

The synthesis, structural, electronic and magnetic characterization of five dinuclear Co(II) azacryptand compounds (**1–5**) bridged through different ions are reported. The magnetic exchange interactions, 2*J* values, obtained from theoretical computations show that the variation of the intermetallic angles and distances lead to antiferromagnetic behaviours. Magneto-structural correlations show a trend, where the angles Co(II)–bridge–Co(II) closer to 180° favour an increase in the superexchange pathway leading to higher AF interaction values.

Introduction

In recent years, the synthesis of compounds containing short ligands with a wide variety of bridging modes to connect metal ions has been the subject of extensive investigation due to their application in many fields including supramolecular chemistry,[1] photoluminescence,[2] catalysis,[3] molecular recognition of important molecules in the biological field,[4] molecular magnetism[5] and environmental fields.[6] From a magnetic point of view, the bridging modes of these ligands can produce a wide range of magnetic behaviours, which range from diamagnetic to moderate or weak antiferromagnetic systems.[7] Furthermore, in some cases these ligands allow antisymmetric interactions (Dzyaloshinski–Moriya interaction, DM), which play a role in canting the spins and minimizing the energy of the system, thereby allowing weak ferromagnetic behaviour to be observed.[8–10] In the past, several research groups have established magneto-structural correlations with first row transition metal compounds, especially with Cu(II);[11–13] however, when there is a significant spin orbital contribution, the correlation becomes difficult to establish. For highly anisotropic ions, such as Co(II), some computational studies of the magnetic moment considering axial splitting and spin–orbit coupling are successful yet limited to mainly mononuclear or very few dinuclear systems in O_h symmetries.[14–17] For polynuclear cases, the type and magnitude of the magnetic exchange interaction depends on many factors, such as the metal–metal separation, the metal–bridging ligand bond lengths, the bridge identity, the dihedral angles between the planes containing the metal ions, the metal ion stereochemistry and the bond angles to the bridging atoms.[18,19]

Consequently, more experimental and computational work with anisotropic systems is essential to establish magneto-structural correlations in order to understand and control the exchange interactions. For this purpose, we decided to use azacryptands ligands, which are known for the ability to modulate their cavity/cage size in order to contain different hosts.[20–22] For transition metals, these ligands lead to dinuclear systems where the metal ions are encapsulated and isolated from the neighbouring molecules, minimizing the intermolecular interactions. At the same time, the molecules can be stabilized

[a]*Centro de Química, Instituto de Ciencias, Universidad Autónoma de Puebla, A.P. 1613, 72000 Puebla, Pue., México*
[b]*Department of Chemistry, University of Ottawa, 10 Marie Curie, Ottawa, Canada K1N6N5. E-mail: m.murugesu@uottawa.ca; Fax: +1(613)562 5170; Tel: +1(613) 562 5800 ext 2733*
[c]*Departamento de Física, Escuela Superior de Física y Matemáticas, I.P.N., Av. Instituto Politécnico Nacional s/n San Pedro Zacatenco, D. F., México 07738*
[d]*Departamento de Física Aplicada, Centro de Investigación de Estudios Avanzados Unidad Mérida. km 6 Antigua carretera a Progreso, Apdo. Postal 73, Cordemex, 97310 Mérida, Yuc., México*
[e]*Department of Chemistry, Indian Institute of Technology Bombay, Mumbai, Powai-400076, India*

† Electronic supplementary information (ESI) available: Crystallographic data for complexes **L1** and **6** (Table S1), selected bond distances and bond angles for **1–5** (Table S2), force constant *k* calculations for **L1** and complexes **1–5** (Table S3), wavelengths and molar absorptivities for electronic transitions in **1–5** (Table S4), overlap integrals calculations for complexes **1–5** (Table S5), contribution to *D* from different spin states for **1–3** (Table S6). X-ray structure of Ligand **L1** (Fig. S1), crystal packing of **4** (Fig. S2), IR spectra of **L1** and complexes **1–5** (Fig. S3), EPR spectra in solution at 77 K for complexes **1–5** (Fig. S4), magneto-structural correlations (Fig. S5), *M vs. H* plots for **1–6** (Fig. S6), DFT fitted χT *vs. T* plots for **1–5** (Fig. S7), MOs of **1–3** (Fig. S8), spin density plots for **1–5** (Fig. S9), 2-dimentional plots for models **1–5** (Fig. S10), X-ray crystallographic information file (CIF) for the structure of ligand **L1** and complexes **1–6**. CCDC 991207–991213. For ESI and crystallographic data in CIF or other electronic format see DOI: 10.1039/c5dt00497g

when the metal ions are linked through a bridging moiety such as an alkyl carbonate bridge formed through a CO_2 fixation process.[23] Mono-, di-, tri-, tetra-, or penta-atomic bridges can be included systematically to replace the alkyl carbonate bridge. This changes the spatial, electronic and magnetic properties of the complex and has been termed "cascade coordination".[24] In this work, we report the synthesis and crystallographic analysis of five Co(II) azacryptand complexes. By varying the nature of the bridging ligands we can influence the structural and electronic properties as well as induce magnetic interactions within each compound as is described in the following sections.

Experimental section

Materials

All chemicals were obtained from commercial sources and used as received, without further purification. "**Caution**! Perchlorate salts of metal complexes with organic ligands are potentially explosive and should be handled with great care."

Ligand synthesis

The ligand 6,16,2,5-tribenzena(1,3)-1,4,8,11,14,18,23,27-octaazabicyclo[9.9.9]nonacosaphane (**L1**) was synthesized by following a modified procedure from the literature.[25] Isophtalaldehyde (15.00 mmol, 2.01 g) and tris(2-aminoethyl)amine (10.00 mmol, 1.46 g) were dissolved in 50 mL of MeOH and refluxed for one hour. A white powder was collected, washed with Et_2O and MeOH and re-dissolved in 200 mL of dried EtOH at reflux, then $NaBH_4$ (26.40 mmol, 1.00 g) was added slowly in small quantities. The mixture was refluxed for 3 hours and left to stir for 36 hours at RT. After this time, the solvent was removed and the product was mixed with 50 mL of a 1 M NaOH solution, extracted with chloroform, washed with water and dried to get a white waxy liquid. Attempts to get the dinuclear Dy(III) compound with **L1** (0.10 mmol, 0.06 g) and $DyCl_3{\cdot}6H_2O$ (0.20 mmol, 0.07 g) in 10 mL of MeOH for 2 h leads to crystallization of **L1** with a protonation of five out of the eight amine groups to ammonium positions with Cl^- as counter ions. The solution obtained was filtered and left to slow evaporation. Yield: 70%. ^{1}H-NMR in $CDCl_3$. δ (ppm): 8.19 (d, 3H), 8.17 (d, 3H), 7.57 (s, 6H), 7.52 (t, 3H), 5.32 (s, 3H), 3.77 (br, 6H), 2.23 (br, 6H), 2.92 (br, 6H), 2.69 (br, 6H). Selected IR (KBr pellet, cm^{-1}): 2814 (br), 2311 (w), 1452 (m), 1332(s), 1279 (s), 1155 (m), 1051 (m), 745 (vs), 699 (s), 656 (m).

Synthesis of $[Co^{II}_2(L1)(OAc)](ClO_4)_3{\cdot}2MeOH$ (1). The slow addition of $Co(ClO_4)_2{\cdot}6H_2O$ (0.20 mmol, 0.07 g) and $(n\text{-}Bu)_4NCH_3CO_2$ (0.20 mmol, 0.06 g) in 5 mL of CH_3CN to **L1** (0.10 mmol, 0.06 g) in 5 mL of MeOH yielded a bright green solution, which was stirred for three hours then filtered. Green rhombic crystals suitable for X-ray measurements were obtained by slow diffusion of Et_2O.[26] Selected IR (KBr pellet, cm^{-1}): 3239 (br), 2876 (br), 1567 (m), 1454 (m), 1068 (vs), 796 (m), 751 (m), 699 (m), 620 (vs). Yield = 40%. UV-Vis (λ in nm/ε in M^{-1} cm^{-1}): 460/230.14, 478/267.47, 602/256.09, 717/86.50.

Synthesis of $[Co^{II}_2(L1)(OCN)](ClO_4)_3{\cdot}2CH_3CN$ (2). The slow addition of $Co(ClO_4)_2{\cdot}6H_2O$ (0.20 mmol, 0.07 g) in 5 mL of CH_3CN and NaOCN (0.20 mmol, 0.01 g) dissolved in the minimum quantity of H_2O to **L1** (0.10 mmol, 0.06 g) in 5 mL of a MeOH yielded to a bright green solution, which was stirred for three hours then filtered. Green rectangular crystals suitable for single crystal X-ray diffraction analysis were obtained by slow diffusion of Et_2O. Selected IR (KBr pellet, cm^{-1}): 3245 (w), 2879 (w), 2277 (m), 1435 (m), 1057 (vs), 790 (w), 753 (m), 697 (w), 620 (vs), 580 (w). Yield = 36%. UV-Vis (λ in nm/ε in M^{-1} cm^{-1}): 458/228.90, 478/221.42, 602/172.25, 707/59.24.

Synthesis of $[Co^{II}_2(L1)(N_3)](N_3){\cdot}(ClO_4)_2{\cdot}H_2O$ (3). The slow addition of $Co(ClO_4)_2{\cdot}6H_2O$ (0.20 mmol, 0.07 g) in 5 mL of CH_3CN and NaN_3 (0.20 mmol, 0.01 g) dissolved in the minimum quantity of H_2O to **L1** (0.10 mmol, 0.06 g) in 5 mL of MeOH yielded to a green solution, which was stirred for three hours then filtered. Green needles suitable for single crystal X-ray diffraction analysis were obtained by slow diffusion of Et_2O. Selected IR (KBr pellet, cm^{-1}): 3591 (br), 3250 (w), 2882 (w), 2193 (vs), 2024 (vs), 1436 (m), 1061 (vs), 794 (m), 755 (m), 700 (vs), 621 (s). Yield = 65%. UV-Vis (λ in nm/ε in M^{-1} cm^{-1}): 461/187.42, 477/177.34, 602/290.19, 696/65.49.

Synthesis of $[Co^{II}_2(L1)(Cl)](ClO_4)_3{\cdot}MeOH$ (4). This complex was obtained following a modified procedure from the literature.[27] The slow addition of $Co(ClO_4)_2{\cdot}6H_2O$ (0.20 mmol, 0.07 g) and $(n\text{-}Bu)_4NCl$ (0.20 mmol, 0.05 g) in 7 mL of CH_3CN to **L1** (0.10 mmol, 0.06 g) in 2 mL of MeOH yielded a purple solution with purple powder, which was stirred for three hours then filtered. The powder was re-dissolved in CH_3CN and purple rhombic crystals suitable for single crystal X-ray measurements were obtained by slow diffusion of Et_2O. The complex obtained in this work contains different solvent molecules within the lattice than those reported in the literature. Selected IR (KBr pellet, cm^{-1}): 3512 (br), 3264 (w), 2946 (br), 1472 (w), 1438 (w), 1284 (w), 1164 (w), 1052 (vs), 1019 (vs), 923 (m), 889 (m), 809 (m), 763 (m), 708 (w), 621 (vs). Yield = 32%. UV-Vis (λ in nm/ε in M^{-1} cm^{-1}): 510/112.07, 609/161.74, 680/54.12, 796/26.75.

Synthesis of $[Co^{II}_2(L1)(Br)](ClO_4)_3{\cdot}MeOH$ (5). The slow addition of $Co(ClO_4)_2{\cdot}6H_2O$ (0.20 mmol, 0.07 g) and $(n\text{-}Bu)_4NBr$ (0.20 mmol, 0.06 g) in 7 mL of CH_3CN to **L1** (0.10 mmol, 0.06 g) in 2 mL of MeOH yielded a purple solution with purple powder, which was stirred for three hours then filtered. The powder was re-dissolved in CH_3CN and purple rhombic crystals suitable for single crystal X-ray measurements were obtained by slow diffusion of Et_2O. Selected IR (KBr pellet, cm^{-1}): 3585 (br), 3248 (br), 2876 (br), 1634 (s), 1453 (m), 1342 (m), 1074 (vs), 801 (s), 756 (s), 700 (s), 621 (s). Yield = 12%. UV-Vis (λ in nm/ε in M^{-1} cm^{-1}): 480/132.56, 606/173.40, 685/126.54, 775/30.13.

Synthesis of $[Co^{II}_2(L1)(MeCO_3)][Co^{II}(NCS)_4]ClO_4{\cdot}CH_3CN$ (6). The slow addition of $Co(ClO_4)_2{\cdot}6H_2O$ (0.20 mmol, 0.07 g) and $(n\text{-}Bu)_4NSCN$ (0.20 mmol, 0.06 g) in 5 mL of CH_3CN to **L1** (0.10 mmol, 0.06 g) in 5 mL of MeOH yielded a bright blue solution, which was stirred for three hours then filtered. After

2 days blue rectangular crystals suitable for single crystal X-ray measurements were obtained by slow diffusion of Et_2O. Selected IR (KBr pellet, cm^{-1}): 3192 (br), 2877 (br), 2061 (vs), 1629 (s), 1456 (m), 1343 (m), 1201 (w), 1073 (m), 800 (m), 757 (m), 701 (m), 622 (m), 568 (br). Yield = 12%.

Magnetic measurements

The variable temperature magnetic susceptibility measurements were obtained using a Quantum Design SQUID MPMS-XL7 magnetometer operating between 1.8 and 300 K and applied dc fields of −7 to 7 T. The analyses were performed on polycrystalline samples of 20.0, 21.9, 9.0, 21.5 and 7.8 mg of compounds **1–5**, respectively, wrapped in a polyethylene membrane. Diamagnetic corrections were applied for the sample holder and the core diamagnetism from the sample (estimated with Pascal constants).

X-ray diffraction

Single yellow needles (**L1**), dark green rectangular (**1–2**), purple rhombic (**3–4**) and blue rectangular (**5–6**) crystals suitable for X-ray diffraction measurements were mounted on a glass fiber. Unit cell measurements and intensity data collections were performed on a Bruker-AXS SMART 1 k CCD diffractometer using graphite monochromatized Mo Kα radiation (λ = 0.71073 Å). The data reduction included a correction for Lorentz and polarization effects, with an applied multi-scan absorption correction (SADABS). The crystal data and refinement parameters for **1–5** are listed in Table 1 and for **L1** and **6** in Table S1.† Selected interatomic distances and angles for complexes **1–5** are listed in Table S2.† The crystal structures are solved and refined using the SHELXTL package.[28] All hydrogen atom positions are calculated geometrically and are riding on their respective atoms.

Computational details

Magnetic coupling constant calculations for all these five complexes have been performed using Gaussian 09 suit of programmes[29] on the X-ray structures. We have employed Noodlemann's broken symmetry[30] approach along with B3LYP[31] functional. All the atoms are described by Ahlrichs-TZV[32] basis set, except the Br atom. The Br atom is treated by an ECP SDD[33] basis set.

This methodology has a proven track record of yielding good numerical estimate of exchange constants.[34] The *g*-tensors and the zero-field splitting (ZFS) parameters are computed using *ab initio* N-electron valence perturbation theory (NEVPT2) method as implemented in ORCA software suit.[35] The *ab initio* calculations generally yield superior estimate of anisotropy compared to density functional theory (DFT) approaches as it has been shown recently.[36] State-average complete active space self-consistent field methods (SA-CASSCF) calculations were performed for each Co(II) ions individually (the other Co(II) in the dinuclear complex is modelled as a Zn(II) ion) incorporating the five d-orbitals and seven electrons in the active space (CAS (7,5) setup). Calculations were carried out with ten quartet and forty doublet excited states in our calculations.[36f] Here we have employed def2-TZVPP basis set for Co(II) and def2-TZVP basis set for the Zn, Br, O and N. For C and H we have used def2-SVP basis set for the ZFS calculations.[37] The calculations utilized the Resolution of Identity (RI) approximation with the auxiliary def2-SVP/C and def2-SV/C Coulomb fitting basis sets and the chain-of spheres (RIJCOSX) approximation to exact exchange as implemented in ORCA. The employed methodology has been used earlier to obtain accurate estimations of the ZFS parameters.[36f,38] To treat the dynamic correlations, NEVPT2 calculations[39] on SA-CASSCF converged wave functions were performed. Since the NEVPT2 correlated

Table 1 Crystallographic data for complexes **1–5**[a]

	1	2	3	4	5
Formula	$C_{40}H_{65}Cl_3Co_2N_8O_{16}$	$C_{39}H_{56}Cl_3Co_2N_{10}O_{13}$	$C_{36}H_{56}Cl_2Co_2N_{14}O_9$	$C_{37}H_{58}Cl_4Co_2N_8O_{13}$	$C_{37}H_{58}BrCl_3Co_2N_8O_{13}$
Fw	1138.21	1097.15	1017.70	1082.57	1127.02
Crystal system	Triclinic	Monoclinic	Orthorhombic	Orthorhombic	Orthorhombic
Space group	$P\bar{1}$	$C2/c$	$Pnma$	$Ama2$	$Ama2$
a/Å	11.8993(4)	39.4302(15)	8.9461(4)	24.1438(5)	24.3318(7)
b/Å	12.1898(5)	9.1554(4)	29.4146(9)	17.6734(3)	17.6327(5)
c/Å	18.1111(6)	30.0283(12)	18.0171(7)	10.6296(2)	10.6002(3)
α/°	101.540(2)	90	90	90	90
β/°	100.071(2)	115.497(2)	90	90	90
γ/°	94.943(2)	90	90	90	90
Vol./Å^3	2514.19(16)	9784.5(7)	4741.1(3)	4532.68(15)	4547.9(2)
Z	2	8	4	4	4
ρ_{calcd}, g cm^{-3}	1.503	1.490	1.426	1.585	1.646
μ (Mo, Kα), mm^{-1}	0.893	0.912	0.877	1.038	1.885
F (000)	1188	4552	2120	2248	2320
Measd/indep	26 583/10 116	66 119/9912	31 955/4081	34 331/5604	36 867/5719
$R_1(I > 2\sigma(I))$	0.0782	0.0789	0.1132	0.0564	0.0584
wR_2 $(I > 2\sigma(I))$	0.1970	0.1862	0.2940	0.1602	0.1638
GOF on F^2	1.039	1.015	1.121	0.886	0.957
CCDC numbers	991207	991208	991209	991210	991211

[a] $R_1 = \sum||F_o| - |F_c||/\sum|F_o|$; w$R_2 = \{\sum w[(F_o)^2 - (F_c)^2]^2/\sum w[(F_o)^2]^2\}^{1/2}$.

energies are found to be more accurate towards the estimation of ZFS parameters,[36b,38a–d,g] here we restricted our analysis to NEVPT2 results. The reported *g*-tensors are also computed using the same methodology.

IR, UV-Vis, NMR and EPR spectroscopy

Infrared analyses were performed using a Nicolet Nexus 6700 FT-IR spectrometer in the 4000–600 cm^{-1} range. UV-Vis spectra were collected on a Shimadzu UV-3100S spectrophotometer in CH_3CN. NMR analyses were conducted on a Bruker Advance 400 spectrometer equipped with an automatic sample holder and a 5 mm auto tuning broadband probe with *Z* gradient. EPR measurements were carried out on polycrystalline samples with a JEOL JES-RES 3X equipment at 300 K and in 15×10^{-4} M CH_3CN solutions at 77 K.

Results and discussion

Synthesis

The synthesis of complexes **1–5** requires 50% excess of the corresponding bridging ligand salt in order to obtain adequate crystals for X-ray measurements. For complex **3**, this excess leads to two different kinds of azide anions: one acting as a bridge between the metal centres, while the other acts as a counter ion of the azacryptand complex.

In a similar way, an excess of the thiocyanate salt, leads to the formation of complex **6** shown in Fig. 1, which consists of a cationic azacryptand dinuclear Co(II) complex linked by a methylcarbonate bridge and a $[Co(NCS)_4]^{2-}$ anionic complex. Harding *et al.* have previously reported dinuclear Cu(II) and Ni(II) compounds with a methylcarbonate ion linking the metallic centers and ClO_4^- as counter ions.[40] It has been proposed that methylcarbonate complexes are obtained in a basic reaction medium by coordination and deprotonation of a water molecule to get a Metal–OH complex, which attacks the electrophilic C atom from an atmospheric CO_2 to form a bicarbonate complex. A subsequent nucleophilic attack from a MeOH solvent molecule and finally a methanolysis reaction leads to the final compound.[41] In compound **6**, the positive charges of the three Co(II) ions are balanced by the methylcarbonate bridge, four SCN^- ions and finally ClO_4^-/SCN^- ions in 50/50% occupancy. For the $[Co(SCN)_4]^{2-}$ complex the Co–N average bond distance is 1.940 Å, the N–Co–N angles vary from 106.12–114.80° and the maximum deviation from linearity in the SCN^- groups is 2.25°, which is indicative of slight distortions from tetrahedral geometry. The $[Co(NCS)_4]^{2-}$ anionic complex interacts with the cationic azacryptand complex by N–H···S hydrogen bonds at an average distance of 2.82 Å, so the closest intermolecular Co···Co distance is 5.90 Å. Despite adding stoichiometric quantities of the thiocyanate salt and changing the reaction conditions, a complex containing a thiocyanate bridge could not be obtained; however, it is possible to obtain complex **2** by using a isocyanate bridge and **3** by using an azide bridge (Fig. 2). This can be explained by the principle of hard and soft acids and bases (HSAB), according to which the borderline acid Co(II) has a tendency to coordinate with hard bases containing highly electronegative O or N donor atoms instead of the soft polarizable bases containing S.[42] Lu *et al.* have reported similar molecular recognition for halogen bridges in which the azacryptand ligand shows affinity towards Cl^- and Br^- ions, but not F^- and I^- ions because of the size matching in the cavity.[27] With these antecedents, the molecular recognition of the azacryptand ligand for transition metals was verified by attempting to use lanthanide ions, which led to the crystallization of the azacryptand as it was described in the synthesis part (Fig. S1†).

Structural analysis

The crystallographic and structural refinement data are presented in Table 1 for compounds **1–5** and in the ESI† for **L1**

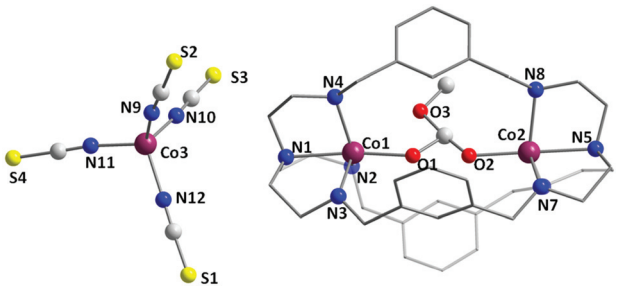

Fig. 1 Molecular structure of compound **6** highlighting the $[Co(NCS)_4]^{2-}$ complex. Colour code: purple (Co), blue (N), red (O), grey (C), yellow (S). Other counter ions and solvent molecules have been omitted for clarity.

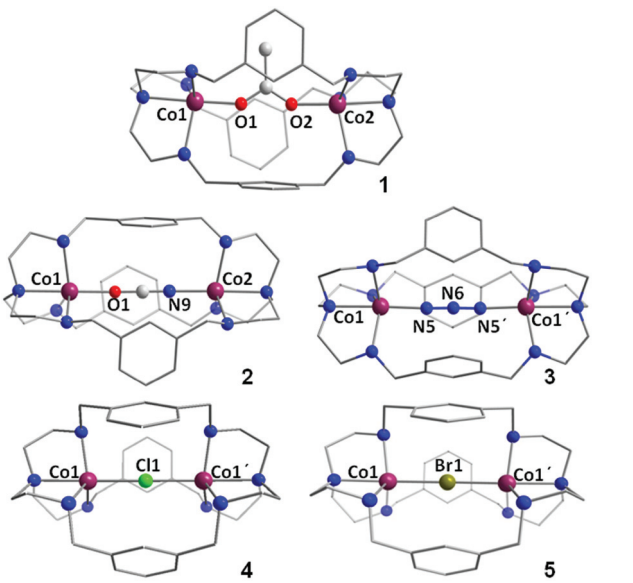

Fig. 2 Molecular structures of complexes **1–5** showing the different bridging ligands. Counter ions, hydrogen atoms and solvent molecules are omitted for clarity. Colour code: purple (Co), blue (N), grey (C), red (O), light green (Cl), dark green (Br).

and **6** (Table S1†). Selected bond lengths and bond angles for all compounds are presented in Table S2.† Since the structural properties of **6** are different from the other five complexes, a direct comparison cannot be achieved; therefore, structural, electronic and magnetic analyses were done for **1–5** only. Fig. 2 shows the X-ray structures of **1–5**, which are dinuclear systems formed by two Co(II) ions coordinated to the N amine atoms of the azacryptand molecule and linked *via* OAc^- (**1**), OCN^- (**2**), N_3^- (**3**), Cl^- (**4**) or Br^- (**5**) ions. Each penta-coordinated Co(II) ion can be described using the parameter τ, which for a perfect square pyramidal geometry (SP) is equal to zero, while for a perfect trigonal-bipyramidal geometry (TBP) it is equal to 1.[43] The τ factors for Co(1)/Co(2) are 0.83/0.65 in **1**, 0.94/0.95 in **2**, 0.85 in **3**, 1.00 in **4** and 0.99 in **5**, indicating geometries very close to the perfect TBP for short and rigid bridges such as OCN^-, Cl^- and Br^-. This occurs when the two azacryptand tertiary amines, the bridging ligand and the two Co(II) ions are almost collinear. As shown in Fig. 2, the rigidity of the azacryptand leads to unusual bridging modes. In the case of compound **1**, the bridging mode can be described as *anti–anti*, which is rarely observed. Most of the complexes containing acetate bridges display the mode *syn–syn* or, in very few cases, *syn–anti*;[44] however the linear position of the OAc^- with the metal ions in compound **1** is the first to be observed so far for cobalt compounds.

Linearity can also be found for the triatomic linear bridges in compounds **2** and **3**, which usually present a *syn* bridging mode.[45,46] A similar compound to **2** containing ClO_4^- as counter ion instead N_3^- has been reported, the difference in the counter ion changes its properties as is shown below.[47] Regarding compounds **4** and **5**, a linear geometry of the halogen bridge with the metallic centres occurs more frequently; however magnetic studies on these complexes are very limited.[48] Careful inspection of the azacryptand conformation in this series of complexes show the ability of the host to optimize the size of the cavity, in order to match the size and shape of the guest ion. The more the guest is sterically demanding and/or has an anisotropic shape, the more the host should allow a large void for accommodating the bridging ion connecting two metal centres. This flexibility is possible because torsion angles around each secondary amine group can be modified through N inversion, affording more or less short arms in each tripodal moiety of the azacryptand. As a consequence, relative benzene planes orientations in the host are related to the nature of the bridging anion. The shortest separation between aromatic rings in symmetry-related molecules is observed at 4.69 Å, with an angle of 54.7° between mean planes of involved rings for. For these interacting rings, the shortest centroid to plane distance is 3.82 Å in **5**, but the same tendency is observed for **4** (Fig. S2b†). For **1–3** parallel-displaced π–π interactions are favoured with closest centroid–centroid distances of 5.407 Å and centroid–plane distances of 3.36 Å. (Fig. S2a†).

For all compounds there are significant interactions between the bridging ligands and the phenyl rings with distances that are shorter than the sum of the van der Waals radii (3.40 Å for C–C, 3.22 Å for C–O and 3.25 Å for C–N, Cl–C 3.45 Å, Br–C 3.55 Å). These interactions are stronger for compounds **4** and **5** with average distances of 3.34 Å for Cl···C in **4** and Br···C in **5**. According to our calculations the non-covalent interactions for these molecules can be considered weak; therefore we conclude that bridge–π interactions are responsible of the molecular arrangement. In order to establish some magneto-structural correlations the Co(1)–Co(2)/Co(1′) intermetallic distances (R), the Co(1)–X–Co(2)/Co(1′) Φ angles (where X = central bridging atom) and the ratio of the distance from the metal ion to the heteroatom in the bridging ligand (R1) and the Φ angles were obtained (Table 2).

Electronic structure analysis

The electronic structure analysis of **1–5** was carried out using IR and UV-Vis spectroscopy. The IR spectra were used to corroborate the formation of the desired compounds through the identification of the characteristic azacryptand, bridging ligands, counter ions and solvents peaks (Fig. S3†).[49] Force constants (k) calculations based on a harmonic oscillator approximation were done for **L1** and for compounds **1–5** (Table S3†). In general, higher values of k are indicative of stronger bonds,[50] k values for the ν(C–H)st and ν(C–H)δ vibration frequencies are higher for compounds **4** and **5** compared to compounds **1–3**. Therefore we conclude that the halogens bridges are acting as electronic density donors as opposed to electron density withdrawing, which is in agreement with the DFT calculations previously reported for azacryptand compounds with halogen bridges.[27] UV-Vis spectra in CH_3CN of **1–5** (Fig. 3) can be divided into two groups since compounds **4** and **5** exhibit an additional peak (Fig. 3, signal i). For high spin Co(II) ions in a TBP field three bands are expected in the visible region around 770 nm, 550 nm and 475 nm for $^4A'_2(^4F) \rightarrow {}^4E'\ (^4F)$, $^4A'_2(^4F) \rightarrow {}^4E''\ (^4P)$ and $^4A'_2(^4F) \rightarrow {}^4A'_2(^4P)$ transitions, respectively.[51] These bands are assigned in **4** and **5** to signals f–i and in **1–3** to signals a–d. The transition $^4A'_2(^4F) \rightarrow {}^4E'\ (^4F)$ is shifted to higher energies for **2** and disappears for **1** and **3** due their distortions from the TBP geometries, as it is indicated by their τ factors. A Gaussians curve analysis was done for each spectrum and the molar absorption coefficient (ε) was calculated for the components of the spectra (Table S4†). The ε values indicate that the signals at the lowest energy (Fig. 3, signals e and j) can be assigned to $^4A'_2(^4F) \rightarrow {}^2E''(^4F)$ spin-forbidden transitions.[51]

The shifting of the bands in **4–5** can be discussed based on the reported spectrochemical series,[52,53] where the order of the increasing energy of transitions must be as follows

$$Br^- < Cl^- < OCN^- < OAc^- \sim N_3^-$$

This order is clearly observed in the transition energies for **1–5**. For **1** and **3** the band energies are very similar indicating that the ligand field strengths for OAc^- and N_3^- are very close. The nephelauxetic effect is also observed in the spectra of **4** and **5**, where the increase of the metal–ligand covalent character associated with the soft halogen donors result in the reduction of the inter-electron repulsions and reduction of the

Table 2 Magnetic, structural and computed data for complexes **1–5**

Complex	$\chi T_{300\ K}$ ($cm^3\ K\ mol^{-1}$)	$\chi T_{2\ K}$ ($cm^3\ K\ mol^{-1}$)	μ_{eff} (μ_B)	$2J^a$ (cm^{-1})	$g_{zz}{}^a$	D^a (cm^{-1})	$g_{avg}{}^a$	E/D^a (cm^{-1})	$2J^b$ (cm^{-1})	$g_{zz}{}^b$	$g_{avg}{}^c$	TIP^b ($cm^{-1} \times 10^{-2}$)	R (Å)	Φ (°)	Φ/R1 (° $Å^{-1}$)	J_{SE} (cm^{-1})	J_{Model},^{a} (cm^{-1})
1	5.01	0.30	6.33	−5.3	2.26 (2.38, 2.48)	−15.9, −25.3	2.25, 2.29	0.20, 0.32			2.19		6.03	158.31	81.26	−0.34	−0.11
2	4.70	1.58	6.13	−1.9	2.21 (2.26, 2.26)	3.6, 3.6	2.23, 2.08	0.31, 0.31			2.17		6.33	177.25	89.25	−0.10	−0.06
3	4.71	0.33	6.14	−5.8	2.25 (2.28, 2.28)	7.4, 7.4	2.22, 2.22	0.13, 0.13			2.20		6.25	176.93	88.99	−0.36	−0.11
4	3.29	0.04	5.12	−54.2	2.19 (2.77, 2.77)	—, —	2.19, 2.19	—, —	−58.02	2.15	2.41	5.7	4.89	179.65	75.99	−2.57	−2.5
5	3.13	0.03	5.00	−75.8	2.17 (2.24, 2.24)	3.39	2.22, 2.22	0.16, 0.16	−71.46	2.19	2.23	6.3	4.73	179.06	73.29	−3.22	−3.0

[a] Computed data. [b] Fitting data. [c] Experimental data.

Fig. 3 UV-Vis spectra of **1–3** (left) and **4–5** (right).

gap energy as it is evidenced by the shifting of the transitions to lower energies.[53–55]

Magnetic measurements

The magnetic properties for all five compounds were measured as polycrystalline samples. Direct current (dc) magnetic susceptibility measurements were performed in the 1.8–300 K temperature range under an applied magnetic field of 1000 Oe. The *g*-tensor and the 2*J* values were computed based on the experimental structures with coordinates directly taken from the X-ray diffraction experiments. Table 2 summarizes the computed and experimental 2*J* and *g* values, the fitting data and other important structural parameters.

The plots of the temperature dependence of the χT product for all five compounds are shown in Fig. 4. Two sets of curves are observed: set I includes triatomic bridge compounds **1–3**, while set II comprises monoatomic bridge compounds **4–5**. For set I the χT product decreases slowly from 300 K to 40 K, then rapidly until 2 K, where the minimum χT values are reached. For set II there is a rapid decreasing of the χT product at higher temperatures indicating antiferromagnetic exchange

Fig. 4 Temperatures dependence of χT product for complexes **1–5**. Solid line represents the fitting for **4–5** (see text).

interactions.[56] Room temperature χT values for set I are higher than the expected spin only value of 3.76 cm^3 K mol^{-1} for two non-interacting high-spin Co(II) (Table 2). Such higher values are often observed in Co(II) systems due to their unquenched first order orbital angular momentum leading to significant spin–orbit coupling contribution.[51]

For set II the χT values at room temperature for **4** and **5** are 3.29 and 3.13 cm^3 K mol^{-1}, respectively, which are close to the spin only value of 3.76 cm^3 K mol^{-1}. Sakiyama *et al.*[51] found that under a pure D_{3h} symmetry, the ground $^4A_2'$ term does not have an orbital angular momentum, rendering the spin-only treatment possible. Based on the structural study **4** and **5** have near perfect trigonal-bipyramidal geometry (TBP) (*vide supra*), although all coordinated atoms are not identical which leads to C_{3v} symmetry, however, for simplification of the fitting we assume it has an idealized D_{3h} symmetry for these two complexes. Then the isotropic spin Heisenberg Hamiltonian $\hat{H} = -2JS_1 \cdot S_2$ can be used to describe the interaction between the nearest neighbours. The magnetic susceptibility data were fitted for two $S_1 = S_2 = 3/2$ sites (eqn (1)) and a temperature-independent paramagnetic (TIP) term was included.[57] To provide accurate D values, computational methods will be employed using the C_{3v} symmetry (*vide infra*)

$$\chi = \left[\frac{N\mu_B{}^2 g^2 S(S+1)}{3k_B T}\right]\left[\frac{2e^{2J/k_B T} + 10e^{6J/k_B T} + 28e^{12J/k_B T}}{1 + 3e^{2J/k_B T} + 5e^{6J/K_B T} + 7e^{12J/K_B T}}\right] + \text{TIP} \quad (1)$$

For **1–3**, the structures are significantly distorted from the D_{3h} symmetry, then the mixture of the $^4E''$ term may bring the orbital momentum into the ground term.[51] Since the magnetic behaviour is strongly affected by the orbital momentum of a ground term, it is necessary to add the zero field splitting contribution to the Hamiltonian, this will be implemented in the computational study for **1–3** (*vide infra*). Fig. 4 shows the fitting for **4–5** as solid lines and the fitting data are shown in Table 2. Experimental powder measurements at 300 K and 77 K are EPR silent, consistent with an integer spin ground state coming from the interaction of two high-spin Co(II) ions.[58] However experiments of **1–5** in frozen glass of CH_3CN solutions at 77 K reduce the spin-lattice relaxation times and the spin–spin intermolecular interactions showing broad signals with average g values (Fig. S4†), which are in good agreement with the computed values.[58]

Hatfield and Hodgson deduced a linear correlation between the J values and Φ bridging angles for isotropic Cu(II) oxo-bridged systems.[59] For **1–5** magneto-structural correlations are difficult to establish due the spin–orbit coupling contribution seen in **1–3**. To find if the magnetic interactions showed some dependence on the structural data the $2J$ computed values obtained from the computational studies were plotted *vs.* the Co(II)–X–Co(II) Φ angles (X = bridging ligand) and the metal–metal R distances (Fig. 5). The $2J$ *vs.* Φ plot does not show a clear correlation; but the plot of $2J$ *vs.* R shows an inverse dependence.

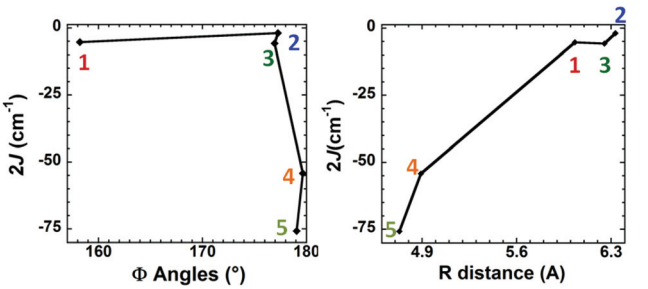

Fig. 5 Plots of $2J$ *vs.* Φ angles (left) and $2J$ *vs.* R distances (right) showing the magneto-structural correlations.

In order to understand the origin of this dependence, theoretical studies were performed showing that the super-exchange pathway *via* the bridge is the dominant interaction. Moriya proposed that when spin–orbit coupling effects are included in the superexchange formalism, the anisotropic superexchange can be approximated by $J_{SE} = J(\Delta g/2)$ (where Δg represents the deviation in the gyromagnetic ratio from the free-electron value of two).[60] The approximated anisotropic superexchange contribution for **1–5** calculated from the computed J and g values through this formula showed that the superexchange mechanism is less significance as the Φ angles become smaller leading to smaller J_{AF} values (Table 2). Therefore, the J_{AF} contribution is given by the superexchange mechanism and the J_F by the direct mechanism. Some other magneto-structural correlations have been established for Cu(II) dinuclear systems compounds by normalizing the Φ angles from the metal–heteroatom distance in the bridging ligand (R1) and plotting the computed $2J$ values *vs.* the Φ/R1 ratio.[61,62] This plot for **1–5** is shown in Fig. S5† and exhibits a similar trend as Fig. 5 with a maximum value of Φ/R1 = 89.25 for **2**, which shows the smallest antiferromagnetic $2J$ value. Below this ratio the increase of the antiferromagnetic coupling constant follows the decrease of the Φ/R1 ratio.

Magnetization measurements were carried out at 1.8 K and 5 K for all five compounds. The M_{mol} *vs.* H plots are shown in Fig. S6† For **2** and **3** there is a linear behaviour of M_{mol} with respect to H; while for **1**, **4** and **5** there is a rapid increase followed by a gradual increase towards a near saturation at $H = 7$ T and $T = 1.8$ K can be observed. The saturation values for **1**, **4** and **5** are 5.35, 0.06 and 0.06 $N\beta$ units, respectively. These values are much lower than the theoretical limit $M = g_{iso}S_{max} = 8.1N\beta$. Such difference can be attributed to the AF coupling for **4** and **5** and to a combination of AF coupling and population of low lying excited states even at low temperatures in **1**.[63] Alternating current (ac) susceptibility measurements were carried out under an oscillating field of 3 Oe, in the absence of an applied dc field as well as under an applied field of 1000 Oe, and frequencies ranging from 0.1–1500 Hz in a range of 2–15 K. No signal was observed in the out-of-phase susceptibility *versus* temperature plot. Absence of ac signal simply precludes any magnet-like behaviour for these dinuclear complexes.

Theoretical studies

In order to probe the effect of different bridging groups on the magnetic coupling constants between two Co(II) metallic centres, we have performed a computational study and results are summarized in Table 2. In all five complexes magnetic interaction is found to be antiferromagnetic in nature as expected for the linear Co–L–Co arrangement. The computed $2J$ values for **4** and **5** correlate with the experimental estimates and also reproduce the experimental χT *vs.* T behaviour (see Fig. S7†). Weak antiferromagnetic exchange for complexes **1–3** and strong antiferromagnetic exchange for complexes **4–5** are observed and this is due to the fact that the super-exchange interactions are mediated through three linker atoms in complexes **1–3** while in complexes **4** and **5**, they are mediated *via* one linker atom.

In complexes **1–5**, there are three exchange pathways: (i) direct exchange through space (ii) superexchange *via* the ligand moiety (iii) superexchange *via* the anionic linker groups. To understand the origin of the interactions further, calculations were done on fictitious model complexes by removing the anionic linker atoms (see Table 2). The obtained $2J_{\text{model}}$ values are weak and are antiferromagnetic in nature. This clearly suggests that the dominant contributions to J's arise from the anionic linker atoms.

Our orbital analysis reveals three interactions between two Co(II) centres namely $d_{xy}|p_x|d_{xy}$, $d_{x^2-y^2}|p_x|d_{x^2-y^2}$ and $d_{z^2}|p_z|d_{z^2}$. Among these three interactions, the interaction *via* the d_{z^2} orbital is found to be significant in all complexes and the computed overlap integral correlates with the magnitude of the J values (see Fig. 6, Fig. S8 and Table S5†). As d_{xy} and $d_{x^2-y^2}$ orbitals are perpendicular to the bridging moiety, their contributions to superexchange mediating through the anion linker are minimal. For complexes **1–3**, the frontier molecular orbitals which interact with the magnetic orbitals of Co(II) are π in character and are in fact perpendicular to the d_{z^2} orbital leading to weak overlap and very small J values (see Fig. S9†).

In complexes **4** and **5** on the other hand the valence s/p_z orbital significantly interacts with the magnetic d_{z^2} orbital, leading to stronger interactions (see Fig. 6). Between complexes **4** and **5**, the larger and more diffuse $5s/4p_z$ orbital of Br overlaps more efficiently than the $4s/3p_z$ orbital of Cl atom leading to larger $2J$ values for complex **5** (see Fig. S8 of ESI†). Stronger delocalization is also evident from the spin density plots, where the following order based on computed spin density on the bridging atoms are found: **5** > **4** > **3** ~ **1** > **2**. This order corresponds to that of the $2J$ values revealing a direct correlation between the spin density at the bridging group and the J values (see Fig. S9 in ESI†). We have calculated intermolecular magnetic coupling constant for complex **2** (using B97D/TZV). The interactions were estimated to have a value of -0.07 cm^{-1} (note the π–π stacking distances here are 3.8 Å). At this stacking distance, we expect the magnetic coupling to be very weak.[64]

Although anisotropy calculations on Co(II) complexes with different coordination spheres have been reported earlier,[36d,f,65] most of the reported Co(II) complexes possess either tetrahedral or octahedral structures. We have calculated the zero-field splitting parameters of complexes **1–3** using ORCA software suite.[35] Although the magnitudes of the computed D values agree well with the experiments in all three cases, the sign of D differs in complex **1**. To further validate the sign of computed D for complex **1**, we have analyzed the susceptibility data and our simulations reveal that it can be fit equally well using both positive and negative D values (see Fig. S10†). This highlights the challenge in obtaining the sign of D from experimental susceptibility data.

The computed ground state electronic configuration for the trigonal bipyramidal Co(II) is found to be $(d_{yz})^2$, $(d_{xy})^2$, $(d_{xz})^1$, $(d_{x^2-y^2})^1$ and $(d_{z^2})^1$. The computed orbital energy levels for complexes **1–3** are shown in Fig. 7. Ideal TBP Co(II) complexes are expected to have two degenerate sets of orbitals: d_{yz}, d_{xz} and d_{xy}–$d_{x^2-y^2}$, and are predicted to yield positive D values.[38e] In

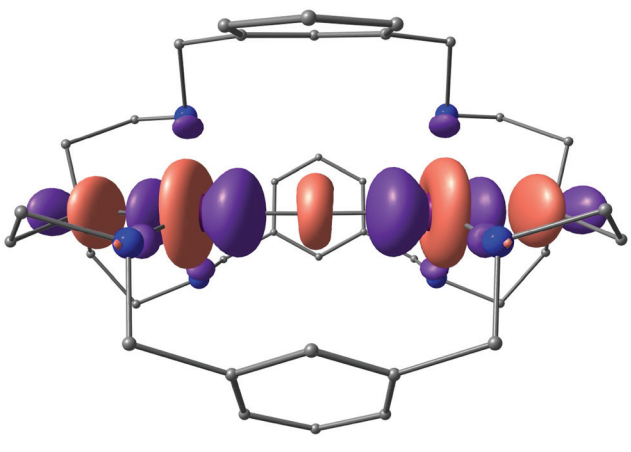

Fig. 6 Molecular orbitals showing dominant $d_{z^2}|p_z|d_{z^2}$ interactions between the two metallic centers in complex **5**.

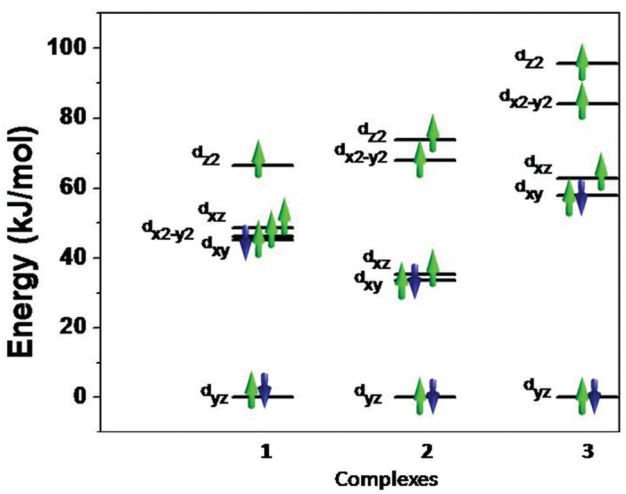

Fig. 7 Computed d-orbitals splitting for complexes **1–3**.

complexes **1–3**, significant distortion from ideal TBP structure is detected and SHAPE analysis[66] reveals that the deviations are 1.97 for complex **1**, 0.54 for complex **2** and 0.82 for complex **3**. In all three complexes, the expected orbital degeneracy for the TBP structure is lifted and deviation from ideal TBP structure is correlated to the magnitude of the *D* values. For complex **1**, the possible contributions to *D* arise from spin-conserved transitions $d_{xy} \rightarrow d_{x^2-y^2}$, $d_{yz} \rightarrow d_{xz}$, $d_{yz} \rightarrow d_{x^2-y^2}$ and $d_{xy} \rightarrow d_{xz}/d_{z^2}$. Here, the first two transitions yield negative contributions to *D* (transitions between same m_l levels) while the other three transitions contribute positive part of *D* value. For complex **1**, the largest contribution arises from the $d_{xy} \rightarrow d_{x^2-y^2}$ transition as the orbitals are very close in energy. The energy of the $d_{x^2-y^2}$ orbital is destabilized in complexes **2** and **3** and significantly reduces the negative *D* contributions in these complexes leading to overall positive *D* values (see Table S6 of ESI†). These transition energies can also be correlated to the experimental absorption spectra discussed earlier. In addition to these complexes, we have also performed calculations on complex **5** where *D* is expected to be smaller as the structure is very close to perfect TBP. Our calculations yield a *D* value of 3.39 cm^{-1}, which is similar to that computed for complex **2** which is also closer to the TBP structure.

Conclusions

Magnetic coupling mediated by a molecular bridge represents one of the fundamental processes that must be considered in the design of new molecular magnetic materials. Thus far, few examples of anisotropic systems allowing the study of the effects of different bridges on the magnetic interactions between metal centres exist. This work shows that structures with geometries very close to perfect TPB have small *D* values, while the distortion of the C_{3v} symmetry brings significant spin–orbit coupling effects and a significant contribution from the direct exchange mechanism. This difference can be observed in the spatial, electronic and magnetic characterization of the compounds, as well as in computational studies. Plots of computed 2*J* values *vs. R* and *vs.* Φ/R1 showed that 2*J* values for **1–5** depend on the *R* distances and the ratio Φ/R1 = 89.25 ° $Å^{-1}$ can be established as the limit value for the smallest antiferromagnetic interaction coupling for this series of dinuclear azacryptand compounds. Our theoretical study provides a clear picture in the nature of the exchange interactions but also provides the origin of the magnetic anisotropy in compounds **1–3**. More experimental and theoretical work is necessary to further our understanding in terms of controlling the exchange interactions in anisotropic systems and efforts are in progress towards that goal.

Conflict of interest

The authors declare no competing financial interest.

Acknowledgements

We thank the University of Ottawa, CFI, NSERC DG, Vanier Canada Graduate Scholarship, Autonomous University of Puebla projects Y-NAT11-I, Y-NAT12-I,Y-NAT13-I and CONACyT Mexico for financial support. Moshinsky Foundation and Conacyt supported the work in Merida. The CGSTIC (Xiuhcoatl) at Cinvestav is gratefully acknowledged for generous allocation of computational resources. GR would like to thank DST, India for its financial support (DST/INT/AUS/P-47/11) and IITB for computational time. MKS thanks UGC for a fellowship.

References

1 F. S. Delgado, C. A. Jiménez, P. Lorenzo-Luis, J. Pasán, O. Fabelo, L. Cañadillas-Delgado, F. Lloret, M. Julve and C. Ruíz-Pérez, *Cryst. Growth Des.*, 2012, **12**, 599–614.
2 M. Nihei, Y. Okamoto, Y. Sekine, N. Hoshino, T. Shiga, I. Po-Chun and H. Oshio, *Angew. Chem., Int. Ed.*, 2012, **51**, 6361–6364.
3 J. Nishigaki, R. Tsunoyama, H. Tsunoyama, N. Ichikuni, S. Yamazoe, Y. Negishi, M. Ito, T. Matsuo, K. Tamao and T. Tsukuda, *J. Am. Chem. Soc.*, 2012, **134**, 14295–14297.
4 (*a*) O. Francesconi, A. Ienco, G. Moneti, C. Nativi and S. Roelens, *Angew. Chem., Int. Ed.*, 2006, **45**, 6693–6696; (*b*) G. Berggren, A. Adamsaka, C. Lambertz, T. R. Simmons, J. Esselborn, M. Atta, S. Gambarelli, J. M. Mouesca, E. Reijerse, W. Lubitz, T. Happe, V. Artero and M. Fontecave, *Nature*, 2013, **499**, 66–69.
5 S. V. Aradhya and L. Venkataraman, *Nat. Nanotechnol.*, 2013, **8**, 399–410.
6 J. Qiu and P. C. Burns, *Chem. Rev.*, 2013, **113**, 1097–1120.
7 (*a*) R. L. Carlin, *Magnetochemistry*, Springer-Verlag, Berlin, 1986; (*b*) P. W. Anderson, *Magnetism*, Academic Press, New York, 1963.
8 C.-M. Liu, S. Gao, D.-Q. Zhang, Y.-H. Huang, R.-G. Xiong, Z.-L. Liu, F.-C. Jiang and D.-B. Zhu, *Angew. Chem., Int. Ed.*, 2004, **116**, 1008–1012.
9 Z. Duan, Y. Zhang, B. Zhang and D. Zhu, *Inorg. Chem.*, 2008, **47**, 9152–9154.
10 Z. Duan, Y. Zhang, B. Zhang and D. Zhu, *J. Am. Chem. Soc.*, 2009, **131**, 6934–6935.
11 O. Kahn, *Angew. Chem., Int. Ed. Engl.*, 1985, **24**, 834–850.
12 W. H. Crawford, H. W. Richardson, J. R. Wasson, D. J. Hodgson and W. E. Hatfield, *Inorg. Chem.*, 1976, **15**, 2107–2110.
13 S. Blügel and G. Bihlmayer, *Magnetism of Low-dimensional Systems: Theory. Handbook of Magnetism and Advanced Magnetic Materials*, Wiley, Germany, 2007.
14 S. Gomez-Coca, E. Cremades, N. Aliaga-Alcalde and E. Ruiz, *J. Am. Chem. Soc.*, 2013, **135**, 7010–7018.
15 A. Jana, S. Konar, K. Das, S. Ray, J. A. Golen, A. L. Rheingold, L. M. Carella, E. Rentsheler, T. K. Modal and S. K. Kumar, *Polyhedron*, 2012, **38**, 258–266.

16 (*a*) M. Radon, M. Srebo and E. Broclawik, *J. Chem. Theory Comput.*, 2009, **5**, 1237; (*b*) T. Matsui, Y. Kitagawa, Y. Shigeta and M. Okumura, *J. Chem. Theor. Comput.*, 2013, **9**, 2974–2980.

17 (*a*) F. Lloret, M. Julve, J. Cano, R. Ruíz-García and E. Pardo, *Inorg. Chim. Acta*, 2008, **361**, 3432–3445; (*b*) J. Húdak, R. Boca, J. Moncol and J. Titis, *Inorg. Chim. Acta*, 2013, **394**, 401–409; (*c*) R. Boca, *Coord. Chem. Rev.*, 2004, **248**, 757–815.

18 J. A. Mccleverty and M. D. Ward, *Acc. Chem. Res.*, 1998, **31**, 842–851.

19 (*a*) X.-Y. Wang, Z.-M. Wang and S. Gao, *Chem. Commun.*, 2008, 281–294; (*b*) R. D. Davy and M. B. Hall, *J. Am. Chem. Soc.*, 1989, **111**, 1268–1275.

20 T. Tozawa, J. Jones, S. Swamy, S. Jiang, D. Adams, S. Shakespeare, R. Clowes, D. Bradshaw, T. Hasell, S. Chong, C. Tang, S. Thompson, J. Parker, A. Trewin, J. Bacsa, A. Slawin, A. Steiner and A. I. Cooper, *Nat. Mater.*, 2009, **8**, 973–978.

21 T. Hasell, W. James, T. A. Jones, J. Bacsa, A. Steiner, T. Mitra, A. Trewin, D. J. Adams and A. I. Cooper, *Nat. Chem.*, 2010, **2**, 750–755.

22 Q. Lu, J. M. Latour, C. J. Harding, N. Martin, D. J. Marrs, V. McKee and J. Nelson, *J. Chem. Soc., Dalton Trans.*, 1994, 1471–1478.

23 (*a*) B. Kersting, *Angew. Chem., Int. Ed.*, 2001, **40**, 3987–3990; (*b*) N. Kitajima, S. Hikichi, M. Tanaka and Y. Moro-oka, *J. Am. Chem. Soc.*, 1993, **115**, 5496–5508; (*c*) M. Rodríguez, A. Llobet, M. Corbella, P. Müller, M.-A. Usón, A. E. Martell and J. Reibenspies, *J. Chem. Soc., Dalton Trans.*, 2002, 2900–2901.

24 J.-M. Lehn, *Pure Appl. Chem.*, 1980, **52**, 2441–2459.

25 (*a*) D. MacDowell and J. Nelson, *Tetrahedron Lett.*, 1988, **3**, 385; (*b*) V. McKee, W. T. Robinson, D. McDowell and J. Nelson, *Tetrahedron Lett.*, 1989, **30**, 7453–7456.

26 Y. Dussart, C. Harding, P. Dalgaard, C. McKenzie, R. Kadirvelraj, V. McKee and J. Nelson, *J. Chem. Soc., Dalton Trans.*, 2002, 1704–1713.

27 J. M. Chen, X. M. Zhuang, L.-Z. Yang, L. Jiang, X. L. Feng and T.-B. Lu, *Inorg. Chem.*, 2008, **47**, 3158–3165.

28 G. M. Sheldrick, *Acta Crystallogr., Sect. A: Fundam. Crystallogr.*, 2008, **64**, 112–122.

29 M. J. Frisch, G. W. Trucks, H. B. Schlegel, G. E. Scuseria, M. A. Robb, J. R. Cheeseman, G. Scalmani, V. Barone, B. Mennucci, G. A. Petersson, H. Nakatsuji, M. Caricato, X. Li, H. P. Hratchian, A. F. Izmaylov, J. Bloino, G. Zheng, J. L. Sonnenberg, M. Hada, M. Ehara, K. Toyota, R. Fukuda, J. Hasegawa, M. Ishida, T. Nakajima, Y. Honda, O. Kitao, H. Nakai, T. Vreven, J. A. Montgomery, J. E. Peralta, F. Ogliaro, M. Bearpark, J. J. Heyd, E. Brothers, K. N. Kudin, V. N. Staroverov, R. Kobayashi, J. Normand, K. Raghavachari, A. Rendell, J. C. Burant, S. S. Iyengar, J. Tomasi, M. Cossi, N. Rega, J. M. Millam, M. Klene, J. E. Knox, J. B. Cross, V. Bakken, C. Adamo, J. Jaramillo, R. Gomperts, R. E. Stratmann, O. Yazyev, A. Austin, J. R. Cammi, C. Pomelli, J. W. Ochterski, R. L. Martin, K. Morokuma, V. G. Zakrzewski, G. A. Voth, P. Salvador, J. J. Dannenberg, S. Dapprich, A. D. Daniels, Ö. Farkas, J. B. Foresman, J. V. Ortiz, J. Cioslowski and D. J. Fox, *Gaussian 09*, 2009.

30 L. Noodleman, D. A. Case and A. Aizman, *J. Am. Chem. Soc.*, 1988, **110**(4), 1001–1005.

31 A. D. Becke, *J. Chem. Phys.*, 1993, **98**, 5648.

32 A. Schäfer, H. Horn and R. Ahlrichs, *J. Chem. Phys.*, 1992, **97**(4), 2571–2577.

33 M. Dolg, U. Wedig, H. Stoll and H. Preuss, *J. Chem. Phys.*, 1987, **86**, 866.

34 (*a*) C. McDonald, S. Sanz, E. K. Brechin, M. K. Singh, G. Rajaraman, D. Gaynor and L. F. Jones, *RSC Adv.*, 2014, **4** (72), 38182–38191; (*b*) N. Berg, T. N. Hooper, J. Liu, C. C. Beedle, S. K. Singh, G. Rajaraman, S. Piligkos, S. Hill, E. K. Brechin and L. F. Jones, *Dalton Trans.*, 2013, **42**(1), 207–216; (*c*) N. Berg, T. Rajeshkumar, S. M. Taylor, E. K. Brechin, G. Rajaraman and L. F. Jones, *Chem. – Eur. J.*, 2012, **18**(19), 5906–5918; (*d*) I. A. Gass, S. Tewary, G. Rajaraman, M. Asadi, D. W. Lupton, B. Moubaraki, G. Chastanet, J.-F. Létard and K. S. Murray, *Inorg. Chem.*, 2014, **53**(10), 5055–5066; (*e*) S. Hazra, S. Bhattacharya, M. K. Singh, L. Carrella, E. Rentschler, T. Weyhermueller, G. Rajaraman and S. Mohanta, *Inorg. Chem.*, 2013, **52**(22), 12881–12892; (*f*) S. Piligkos, H. Weihe, E. Bill, F. Neese, H. El Mkami, G. M. Smith, D. Collison, G. Rajaraman, G. A. Timco and R. E. P. Winpenny, *Chem. – Eur. J.*, 2009, **15**(13), 3152–3167; (*g*) A. Upadhyay, J. Rajpurohit, M. Kumar Singh, R. Dubey, A. Kumar Srivastava, A. Kumar, G. Rajaraman and M. Shanmugam, *Chem. – Eur. J.*, 2014, **20**(20), 6061–6070; (*h*) E. Ruiz, S. Alvarez, A. Rodriguez-Fortea, P. Alemany, Y. Pouillon and C. Massobrio, in *Magnetism: Molecules to Materials II*, ed. J. S. Miller and M. Drillon, Wiley-VCH, Weinheim, 2001, pp. 227–280.

35 F. Neese, *WIREs Comput. Mol. Sci.*, 2012, **2**(1), 73–78.

36 (*a*) D. Gatteschi, R. Sessoli and J. Villain, *Molecular Nanomagnets*, Oxford University Press, New York, 2006; (*b*) M. Atanasov, P. Comba, S. Helmle, D. Müller and F. Neese, *Inorg. Chem.*, 2012, **51**(22), 12324–12335; (*c*) S. K. Singh and G. Rajaraman, *Chem. – Eur. J.*, 2014, **20** (18), 5214–5218; (*d*) S. Vaidya, A. Upadhyay, S. K. Singh, T. Gupta, S. Tewary, S. K. Langley, J. P. S. Walsh, K. S. Murray, G. Rajaraman and M. Shanmugam, *Chem. Commun.*, 2015, **51**, 3739–3742; (*e*) S. Petit, G. Pilet, D. Luneau, L. Chibotaru and L. Ungur, *Dalton Trans.*, 2007, 4582; (*f*) R. Herchel, L. Váhovská, I. Potočňák and Z. Trávníček, *Inorg. Chem.*, 2014, **53**(12), 5896–5898; (*g*) S. K. Singh, T. Gupta, P. Badkur and G. Rajaraman, *Chem. – Eur. J.*, 2014, **20**(33), 10305–10313.

37 F. Weigend and R. Ahlrichs, *Phys. Chem. Chem. Phys.*, 2005, **7**, 3297.

38 (*a*) J. Cirera, E. Ruiz, S. Alvarez, F. Neese and J. Kortus, *Chem. – Eur. J.*, 2009, **15**, 4078–4087; (*b*) F. Neese, *J. Am. Chem. Soc.*, 2006, **128**, 10213; (*c*) F. Neese and E. I. Solomon, *Inorg. Chem.*, 1998, **37**, 6568; (*d*) D. Maganas, S. Sottini, P. Kyritsis, E. J. J. Groenen and

F. Neese, *Inorg. Chem.*, 2011, **50**, 8741; (*e*) S. Gomez-Coca, E. Cremades, N. Aliaga-Alcade and E. Ruiz, *J. Am. Chem. Soc.*, 2013, **135**, 7010; (*f*) E. Cremades and E. Ruiz, *Inorg. Chem.*, 2011, **50**(9), 4016–4020; (*g*) S. Ye and F. Neese, *J. Chem. Theory Comput.*, 2012, **8**(7), 2344–2351; (*h*) R. Maurice, R. Bastardis, C. de Graaf, N. Suaud, T. Mallah and N. Guihéry, *J. Chem. Theory Comput.*, 2009, **5**, 2977; (*i*) R. Maurice, C. d. Graaf and N. Guihery, *Phys. Chem. Chem. Phys.*, 2013, **15**(43), 18784–18804; (*j*) R. Maurice, L. Vendier and J.-P. Costes, *Inorg. Chem.*, 2011, **50**(21), 11075–11081.

39 (*a*) C. Angeli, R. Cimiraglia, S. Evangelisti, T. Leininger and J. P. Malrieu, *J. Chem. Phys.*, 2001, **114**, 10252; (*b*) C. Angeli, R. Cimiraglia and J. P. Malrieu, *Chem. Phys. Lett.*, 2001, **350**, 297; (*c*) C. Angeli, R. Cimiraglia and J. P. Malrieu, *J. Chem. Phys.*, 2002, **117**, 9138; (*d*) C. Angeli, S. Borini, M. Cestari and R. Cimiraglia, *J. Chem. Phys.*, 2004, **121**, 4043.

40 C. J. Harding, Q. Lu, J. F. Malone, D. J. Marrs, N. Martin, V. McKee and J. Nelson, *J. Chem. Soc., Dalton Trans.*, 1995, 1739–1747.

41 B. Kersting and G. Steinfeld, *Inorg. Chem.*, 2002, **41**, 1140–1150.

42 (*a*) R. G. Pearson, *J. Chem. Educ.*, 1968, **45**, 581–587; (*b*) R. G. Pearson, *J. Chem. Educ.*, 1968, **45**, 643–648.

43 A. W. Addison and R. Nageswara, *J. Chem. Soc., Dalton Trans.*, 1984, 1349–1356.

44 (*a*) M. Kruck, D. C. Sauer, M. Enders, H. Wadepohl and L. H. Gade, *Dalton Trans.*, 2011, **40**, 10406–10415; (*b*) V. Mishra, F. Lloret and R. Mukherjee, *Inorg. Chim. Acta*, 2006, **359**, 4053–4062; (*c*) B. K. Langlotz, J. Lloret, J. H. Gross, H. Wadepohl and L. Gade, *Chem – Eur. J.*, 2008, **14**, 10267–10279.

45 (*a*) S. Buchler, F. Meyer, E. Kaifer and H. Pritzkow, *Inorg. Chim. Acta*, 2002, **337**, 371–386; (*b*) S. Derossi, P. T. Farrell, C. J. Harding, V. McKee and J. Nelson, *Dalton Trans.*, 2007, 1762–1772; (*c*) Effendy, C. DiNicola, M. Fianchini, C. Pettinari, B. W. Skelton, N. Somers and A. H. White, *Inorg. Chim. Acta*, 2005, **358**, 763–795.

46 (*a*) F. Meyer, K. Heinze, B. Nuber and L. Zsuinai, *J. Chem. Soc., Dalton Trans.*, 1998, 207; (*b*) W. P. Fehlhammer and W. Beck, *Z. Anorg. Allg. Chem.*, 2013, **639**, 1053.

47 A. Escuer, C. J. Harding, Y. Dussart, J. Nelson, V. McKee and R. Vicente, *J. Chem. Soc., Dalton Trans.*, 1999, 223–229.

48 (*a*) M. R. Kember, F. Jutz, A. Buchard, A. J. P. White and C. Williams, *Chem. Sci.*, 2012, **3**, 1245–1255; (*b*) S. Yuan, S. Bai, H. Tong, X. Wei, D. Liu and W. H. Sun, *Inorg. Chim. Acta*, 2011, **370**, 215–221; (*c*) F. Meyer, K. Heinze, B. Nuber and L. Zsolnai, *J. Chem. Soc., Dalton Trans.*, 1998, 207–213.

49 K. Nakamoto, *Infrared and Raman Spectra of Inorganic and Coordination Compounds*, John Wiley and Sons, New York, 1999.

50 R. Drago, *Physical Methods for Chemists*, Saunders College Pub, New York, 1992.

51 (*a*) M. Jamil and H. Sakiyama, *Inorg. Chim. Acta*, 2002, **338**, 255–259; (*b*) L. Sacconi, M. Ciampolini and G. P. Speroni, *J. Am. Chem. Soc.*, 1965, **87**, 3102–3106.

52 (*a*) P. M. Suh, J. Lee, M. Y. Han and T. S. Yoon, *Inorg. Chem.*, 1997, **36**, 5651–5654; (*b*) G. S. Siluvai and N. N. Murthy, *Inorg. Chim. Acta*, 2009, **362**, 3119–3126.

53 P. W. Atkins, T. L. Overton, J. P. Rourke, M. T. Weller and F. A. Armstrong, *Inorganic Chemistry*, Oxford University Press, New York, 2010.

54 R. Stranger, K. L. McMahon, L. R. Gahan, J. I. Bruce and T. W. Hambley, *Inorg. Chem.*, 1997, **36**, 3466–3475.

55 W. H. Crawford, H. W. Richardson, J. R. Wasson and D. J. Hodgson, *Inorg. Chem.*, 1976, **15**, 2107–2110.

56 P. W. Anderson, *Magnetism*, Academis Press, New York, 1963.

57 E. Shurdha, C. E. Moore, A. L. Rheingold and J. S. Miller, *Inorg. Chem.*, 2011, **50**, 10546–10548.

58 J. H. Rodriguez, D. E. Wheeler and J. K. McCusker, *J. Am. Chem. Soc.*, 1998, **120**, 12051–12068.

59 O. Kahn, *Molecular Magnetism*, VCH Publishers Inc., New York, 1993.

60 T. Moriya, *Phys. Rev.*, 1960, **120**, 91.

61 J. Lalena and D. A. Cleary, *Principles of Inorganic Materials Design*, *John* Wiley and Sons Inc., New York, 2010.

62 R. D. Willet, *Magneto-Structural Correlations in Exchanged Coupled Systems*, Reidel Publishing Company, New York, 1985.

63 J. Hudak, R. Boca, J. Moncol and J. Titis, *Inorg. Chim. Acta*, 2013, **394**, 401–409.

64 M. K. Singh and G. Rajaraman, *Chem. – Eur. J.*, 2015, **21**, 980–983.

65 (*a*) S. Petit, G. Pilet, D. Luneau, L. F. Chibotaru and L. Ungur, *Dalton Trans.*, 2007 (40), 4582–4588; (*b*) J. M. Zadrozny and J. R. Long, *J. Am. Chem. Soc.*, 2011, **133**, 20732; (*c*) T. Jurca, A. Farghal, P.-H. Lin, I. Korobkov, M. Murugesu and D. S. Richeson, *J. Am. Chem. Soc.*, 2011, **133**(40), 15814–15817.

66 M. Llunell, D. Casanova, J. Cirera, J. M. Bofill, P. Alemany, S. Alvarez, M. Pinsky and D. Avnir, *SHAPE*, Universitat de Barcelona and The Hebrew University of Jerusalem, Barcelona, 2003.